Korean Journal of Chemical Engineering (2024) 41:539–544
https://doi.org/10.1007/s11814-024-00117-1

ORIGINAL ARTICLE

Optimizing Molecular Weight of Polyethylene Glycol as an Additive for Stabilizing Zn Metal Anode in Aqueous Electrolyte

Ohhyun Kwon[1] · Jihyeon Kang[1] · Seohyeon Jang[1] · Hojong Eom[1] · Seyoung Choi[1] · Junhyeop Shin[1] · Jongkwon Park[1] · Hyeonjong Seo[1] · Jae Hyun Kim[1] · Soomin Park[2] · Inho Nam[1]

Received: 26 August 2023 / Revised: 11 September 2023 / Accepted: 17 September 2023 / Published online: 14 February 2024

Abstract

Polyethylene glycol (PEG) additives have attracted significant attention as a cost-effective approach for modifying the deposition behavior of Zinc (Zn) anodes. In this study, we investigated the effectiveness of PEG additives in 1 M $ZnSO_4$ aqueous electrolytes, specifically examining the effect of PEG molecular weight on Zn deposition. By exploring the adsorption of PEG polymers with different molecular weights, we identified the PEG with a molecular weight of 300 g mol^{-1} (PEG300) as the most suitable polymer. In terms of electrochemical performance, Zn anodes exhibited steady cycling for 232 cycles with high reversibility in 1 M $ZnSO_4$ electrolyte with 0.1 wt.% PEG300. By contrast, Zn anodes using the control electrolyte of 1 M $ZnSO_4$ began to fail after only 70 cycles. These findings highlight the potential of PEG300 as a simple and adaptable additive for significantly extending the longevity of Zn metal anodes.

Keywords Aqueous Zn ion batteries (ZIBs) · Zn metal anode · Polyethylene glycol (PEG) addictive · Metal dendrite · Surface corrosion

Introduction

Developing stable aqueous batteries represents an effective strategy to address the concerns surrounding safety and cost associated with dominant nonaqueous lithium-ion batteries, which are currently prevalent in the market [1]. Among these, aqueous Zinc ion batteries (ZIBs) stand out as one of the most promising materials owing to their environmental friendliness [2], abundant natural resources [3], high theoretical capacity (820 mAh g^{-1}) [4], and low potential (0.76 V vs. standard hydrogen electrode) [5]. Despite the advantages, numerous challenges such as rampant dendrite growth [6], dead Zn accumulation [7], and corrosion hinder their practical usage [8]. Consequently, enhancing the electrochemical performance of the Zn anode is crucial for further advancements in ZIBs.

Several strategies have been proposed to enhance the durability and performance of Zn anodes in aqueous ZIBs. These strategies include surface/interface adjustments [9–11], electrode/host structure design [12, 13], electrolyte optimization [14–16], and separator modifications [17, 18]. Among these, electrolyte optimization is particularly promising and encompasses the use of high-concentration electrolytes [19, 20], quasi/solid-state electrolytes [21, 22], and electrolyte additives [23, 24]. Electrolyte additives are considered highly advantageous for stabilizing Zn anodes owing to their simplicity, high efficiency, and cost-effectiveness. The deposition of Zn^0 on the anode requires overcoming the desolvation energy barrier of Zn^{2+}, which plays a crucial role in determining transfer kinetics and electrochemical capacity [25]. In this context, electrolyte additives represent a promising approach to facilitate the deposition of Zn^{2+} and improve the electrochemical performance of Zn anodes in advanced energy materials for aqueous ZIBs.

Polyethylene glycol (PEG) has emerged as a highly promising and extensively studied material in recent research for

✉ Soomin Park
smpark@koreatech.ac.kr

✉ Inho Nam
inhonam@cau.ac.kr

[1] Department of Intelligent Energy and Industry, Department of Advanced Materials Engineering, School of Chemical Engineering and Materials Science, Chung-Ang University, Seoul 06974, Republic of Korea

[2] School of Energy, Materials and Chemical Engineering, Korea University of Technology and Education, Cheonan 31253, Republic of Korea

its potential as an electrolyte additive in Zn anodes [26–30]. PEG has demonstrated effective stabilization of the Zn electrode–electrolyte interface through interactions facilitated by the ether groups present in the PEG polymer and Zn^{2+} ions [31]. Previous studies have highlighted the role of PEG as an electrolyte additive, showcasing its ability to form a compact and stable solid electrolyte interphase layer that effectively curbs dendrite growth and reduces electrolyte consumption during cycling [32]. Furthermore, PEG mitigates hydrogen evolution because of its abundant ether groups, which readily bond with free water molecules [26]. However, previous research did not focus on the relationship between the behavior of PEG and its molecular weight, employing varying molecular weights of PEG without establishing a specific optimum value. Thus, a better understanding of methods to strategically modulate the interactions between Zn^{2+} ions and the PEG additive according to its molecular weight is required, which can aid in fine-tuning the reaction kinetics and stability of the Zn anode within dilute aqueous Zn salt electrolytes.

In this work, we investigated the impact of the molecular weight of PEG on the electrochemical performance of the Zn anode by employing PEG-containing electrolytes. PEG with an average molecular weight of 300 g mol^{-1} (PEG300) exhibited remarkable cyclic stability, attracting significant attention. Unlike conventional water solvents, the addition of PEG300 enables its active participation in the Zn^{2+} solvation structure, disrupting hydrogen bonds and meeting the stability requirements for Zn anode in aqueous ZIB (Fig. 1). Even a minute addition of PEG300 in aqueous $ZnSO_4$ not only facilitates the uniform deposition of Zn^{2+} by adjusting the growth orientation but also mitigates the side-reactions on the Zn surface. Consequently, a Zn || Cu cells using 0.1 wt.% PEG300 additive exhibited an unprecedentedly stable long-term cycling performance lasting over 464 h under a current density of 1 mA cm^{-2} with an areal capacity of 1 mAh cm^{-2}.

Experimental Section

The aqueous electrolytes were prepared by mixing 0.1 wt.% PEG with average molecular weights of 200, 300, 400, and 600 g mol^{-1} into 1 M $ZnSO_4$ aqueous solutions. The solutions were stirred at room temperature until the PEG polymer completely dissolved. Zn foil with a thickness of 0.25 mm (Alfa Aesar) punched into 14-mm-diameter disks. The morphology of the electrodes was visualized using scanning electron microscopy (FE-SEM, Carl Zeiss, SIGMA 300). Further, the structure of molecular chains and the chemical environment of atoms were examined using nuclear magnetic resonance (NMR, Bruker AVANCE III HD 500 MHz spectrometer). D_2O solution including the indicator compounds was prepared. Trace amounts of Trimethylsilylpropanoic acid (TSP) was used as internal chemical shift references.

Cu || Zn coin cells were assembled to evaluate the coulombic efficiency (CE) of Zn anodes using different electrolytes. The working electrode was made of Cu foil, the counter electrode was Zn foil, and a glass fiber separator (Whatman, GF D) with a thickness of 0.67 mm and pore size of 2.7 µm was utilized. Cycling tests of Cu || Zn cells were conducted at a constant current density of 1 mA cm^{-2} for extended cycling, with the charging cutoff voltage set at 0.6 V vs. Zn/Zn^{2+}. A battery cycler (WonATech, WBCS-3000) was utilized for the experiments, which were conducted at 25 °C. To investigate the rate performance, Zn || Zn symmetric cells were tested at currents of 1, 3, 5, 10, and 20 mA cm^{-2}, each with an areal capacity of 1 mAh cm^{-2}. Before testing the rate performance, activation cycles (five times) were performed at a current of 0.1 mA cm^{-2} with an areal capacity of 0.1 mAh cm^{-2}. For hydrogen evolution reaction testing, linear sweep voltammetry measurements were carried out using a potentiostat (WonATech, ZIVE SP1), with stainless steel electrodes serving as both working

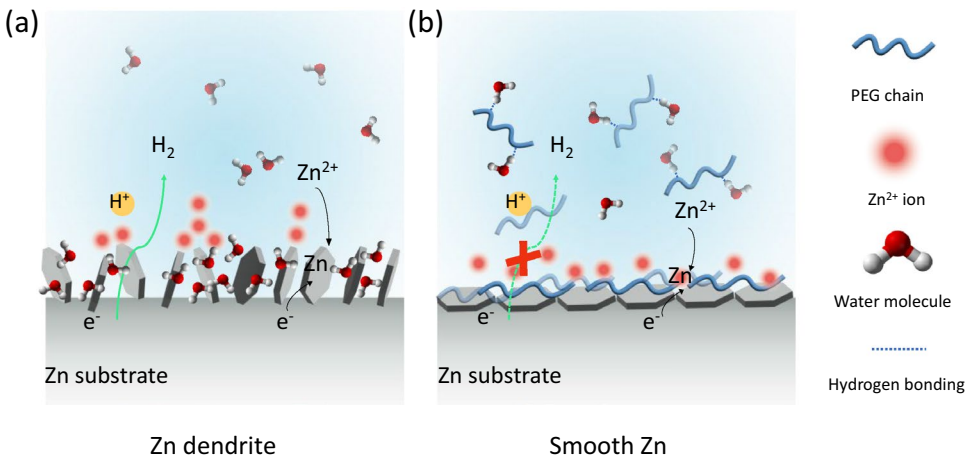

Fig. 1 Schematic representation of Zn deposition in aqueous Zn^{2+} containing electrolytes. **a** Dendritic Zn deposition with concurrent H_2 evolution and **b** smooth Zn deposition with suppressed H_2 evolution under an electrolyte with PEG additive

and counter electrodes, and Zn metal as the reference electrode. The measurements were performed at a scan rate of 5 mV s^{-1} across a voltage range of 0.5 to − 0.4 V vs. Zn/Zn^{2+}. The aqueous solutions contained 0.1 wt.% PEG with different molecular weights (200, 300, 400, and 600 g mol^{-1}) and a PEG-free solution with 1 M Na_2SO_4 as the supporting salt. Exchange current densities were determined by fitting Tafel plots for Zn ‖ Zn symmetric coin cells with a scan rate of 5 mV s^{-1} and a voltage range of − 0.4 to 0.4 V by utilizing a potentiostat (WonATech, ZIVE SP1). In addition, double-layer capacitance measurements were performed on Zn ‖ Zn symmetric coin cells using a potentiostat (WonATech, ZIVE SP1). Different scan rates ranging from 4 to 20 mV s^{-1} were employed, covering a voltage range of − 0.0151 to 0.0151 V.

Result and discussion

To investigate the influence of the molecular weight of PEG on the CE and cycling stability of Zn anodes, we conducted a cycling test using Cu ‖ Zn cells at a constant current density of 1 mA cm^{-2} and an areal capacity of 1 mAh cm^{-2} (Fig. 2a). The electrolytes comprised 1 M $ZnSO_4$ aqueous solutions with 0.1 wt.% PEG (with varying molecular weights: 200, 300, 400, and 600 g mol^{-1}) as additives. For simplicity, we have used the abbreviations PEG200, PEG300, PEG400, and PEG600 to denote PEG with average molecular weights of 200, 300, 400, and 600 g mol^{-1}, respectively.

Zn anodes in pure 1 M $ZnSO_4$ electrolyte exhibited a high CE, exceeding 99.5%, indicating excellent reversibility during Zn deposition and dissolution with a minimal voltage hysteresis of 30 mV (Fig. 2b). These results suggest that the Zn deposition–dissolution process in pure electrolytes exhibits intrinsic high reversibility and rapid kinetics. Despite these favorable characteristics, the Cu ‖ Zn cell experienced rapid short-circuiting after approximately 70 cycles due to intensified heterogeneous growth of the Zn anode during cycling. Zn deposition bumps were observed on the Cu electrodes, and in some cases, these bumps had already penetrated the glass fiber, potentially leading to short circuit in the Cu ‖ Zn cells.

By contrast, the addition of 0.1 wt.% PEG remarkably enhanced the stability of the Zn anode by over threefold. The CE of the electrolyte containing PEG additive increased substantially with increasing molecular weight. This finding aligns with that of a prior study that demonstrated the stabilizing effect of PEG polymer additive on the Zn anode [33]. However, upon the addition of 0.1 wt.% PEG into the 1 M

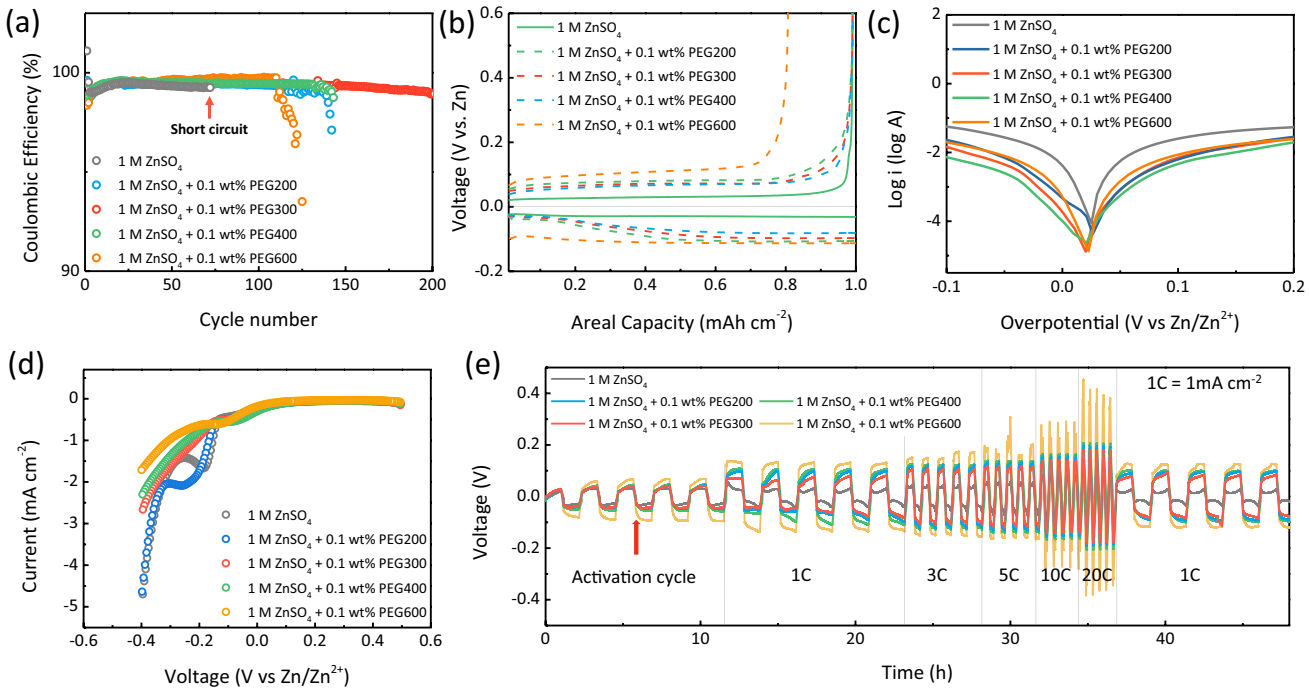

Fig. 2 Electrochemical performance of Zn anodes with various electrolyte compositions. **a** Coulombic efficiency and cycling stability of Zn in Cu ‖ Zn cells with a constant current density of 1 mA cm^{-2} and an areal capacity of 1 mAh cm^{-2}. **b** Voltage profiles of the fifth deposition–dissolution cycle in aqueous $ZnSO_4$ electrolytes with PEG additives of different molecular weights. **c** Tafel plots for Zn deposition–dissolution in aqueous $ZnSO_4$ electrolyte measured from a Zn ‖ Zn symmetric cell. **d** Linear sweep voltammetry data for hydrogen evolution reaction testing using stainless steel as both the working and counter electrodes and Zn as the reference electrode. Measurements were conducted in H_2O with 1 M Na_2SO_4 supporting salt. **e** Galvanostatic cycling of the Zn ‖ Zn symmetric cell symmetric cell using aqueous $ZnSO_4$ electrolytes with and without PEG additives under varying current densities with an areal capacity of 1 mAh cm^{-2}

$ZnSO_4$ electrolyte, a notable increase in voltage hysteresis during Zn deposition–dissolution was observed, rising from 60 to 70, 80, and 90 mV, as shown in Fig. 2b. The increase in overpotential is dependent on the molecular weight of PEG, resulting from a decrease in ionic conductivity due to increased viscosity. Therefore, finding the optimal PEG molecular weight is crucial for achieving a stable and high-performance Zn anode.

Further investigations were conducted to explore the electrochemical interface properties between Zn anodes and aqueous electrolytes. Tafel plots were acquired to evaluate the corrosion-inhibiting role of PEG additives with different molecular weights. The Tafel plot shown in Fig. 2c reveals that the use of PEG additives increases the corrosion potential compared to the 1 M $ZnSO_4$ aqueous electrolyte. A higher corrosion potential is generally associated with a lower tendency for corrosion [34, 35]. Figure 2d displays the hydrogen evolution potentials observed in the linear sweep voltammetry data. The formation of hydrogen bonds between abundant ethereal oxygen atoms in higher-molecular-weight (≥ 300 g mol^{-1}) PEGs and H_2O molecules inhibits the decomposition of H_2O [18], leading to a more pronounced hydrogen evolution-inhibiting property. However, with its low molecular weight, PEG200 exhibits limited ability to form robust hydrogen bonds, resulting in a reduced interaction with H_2O molecules. Moreover, 1 M Na_2SO_4 was utilized as the supporting salt to prevent any potential interference from the Zn deposition current in Zn salt electrolytes.

The rate performance of Zn anodes in electrolytes with different molecular weights of PEG is presented in Fig. 2e. Further, the voltage profiles during Zn deposition–dissolution in 1 M $ZnSO_4$ + 0.1 wt.% PEG electrolyte, tested at current densities ranging from 1 to 20 mA cm^{-2} and an areal capacity of 1 mAh cm^{-2}, are shown in Fig. 2e. The voltage hysteresis of 1 M $ZnSO_4$ electrolyte is consistently below that of PEG additive electrolytes at various current densities. The presence of dense and divalent SO_4^{2-} anions leads to an increase in the solvation energy of Zn^{2+} ions, facilitating a more stable adsorption of PEG polymer on the Zn anode. This enhanced interaction between Zn^{2+} ions and the PEG polymer in the 1 M $ZnSO_4$ + PEG electrolyte is responsible for the phenomenon. The incorporation of PEG polymers was found to induce a substantial increase in overpotential. However, the potential profiles in PEG additive electrolytes exhibited significant difference. Specifically, the 0.1 wt.% PEG300 additive acted as a surface-protective layer that established a connection between H_2O and the hydroxyl group in PEG300 molecules. Furthermore, the absence of potential increase at the end of the dissolution process provided evidence of an intact interphase layer without any deconstruction, indicating no additional consumption of fresh Zn.

To obtain deeper insight into the role of PEG additives during the electrochemical Zn deposition process, NMR was employed to discern the molecular-level interactions between various PEG molecular weights and aqueous electrolytes (Fig. 3a). The ^1H NMR spectra of the ether groups ($–CH_2–O–CH_2–$) in the PEG polymer exhibited a upfield chemical shift in $ZnSO_4$ aqueous electrolytes [36]. In 1 M $ZnSO_4$ electrolytes, a decrease in PEG molecular weight led to a more pronounced upfield chemical shift in the ^1H NMR peak, indicating that PEG molecules were primarily engaged in coordinating with Zn^{2+} cations at lower molecular weights, notably around 300 g mol^{-1}. The interactions between PEG and Zn^{2+} ions within the aqueous $ZnSO_4$ electrolyte demonstrated significant efficacy in modulating the reaction kinetics of Zn^{2+} ion distribution at the interfaces of the Zn anode and the electrolyte. This effect resulted in stable interfacial reactions and a seamless Zn deposition

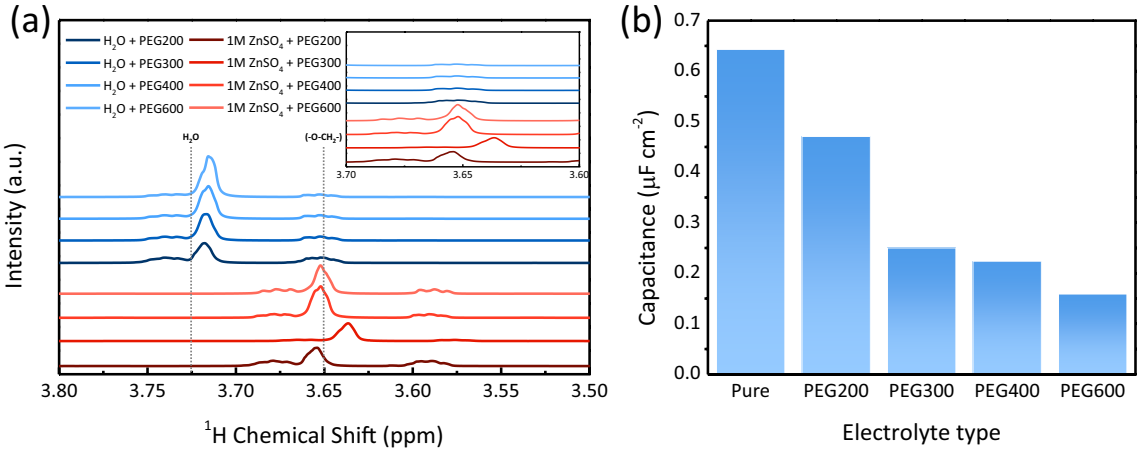

Fig. 3 **a** ^1H NMR data of aqueous $ZnSO_4$ electrolytes with PEG of different molecular weights. **b** Double-layer capacitance at the Zn anode–electrolyte interfaces. Measurements were conducted using 1 M $ZnSO_4$ electrolytes with and without PEG of different molecular weights

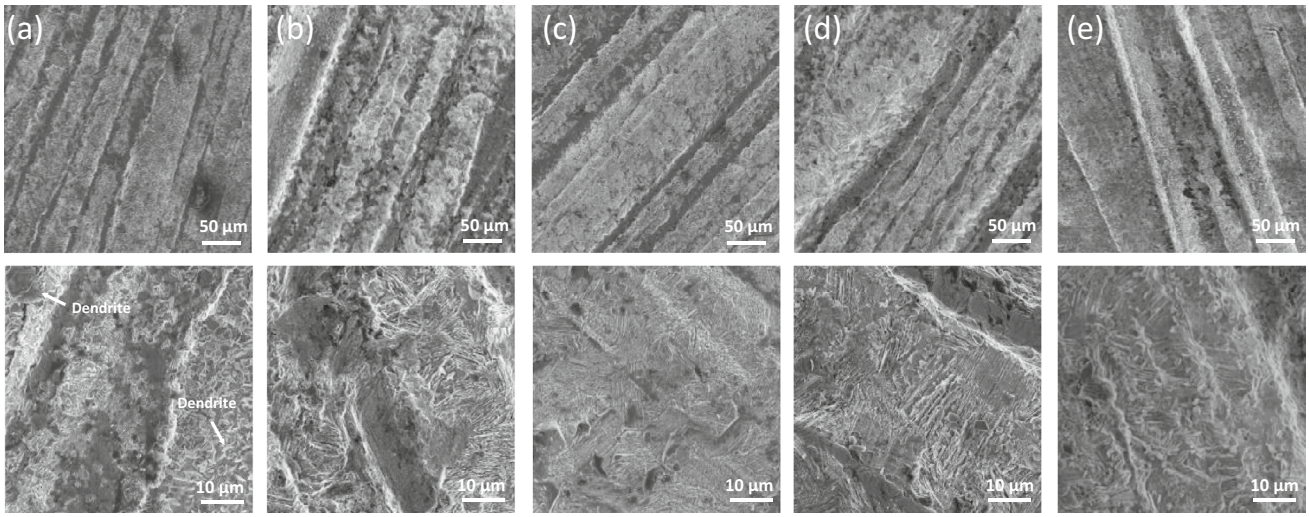

Fig. 4 SEM images of the Zn anode after 20 cycles of deposition–dissolution in a 1 M $ZnSO_4$ electrolyte with and without PEG additives, measured at a current density of 1 mA cm^{-2} and an areal capacity of 1 mAh cm^{-2}. Aqueous electrolyte conditions: **a** 1 M $ZnSO_4$, **b** 1 M $ZnSO_4$ + 0.1 wt.% PEG200, **c** 1 M $ZnSO_4$ + 0.1 wt.% PEG300, **d** 1 M $ZnSO_4$ + 0.1 wt.% PEG400, and **e** 1 M $ZnSO_4$ + 0.1 wt.% PEG600

process. However, the ^{1}H NMR peak (~3.7 ppm) is shifted downfield for molecular weights above 300, indicating the presence of unbound PEG molecules that could enhance interfacial resistance. Therefore, choosing the proper molecular weight is a critical factor for long-term stable cycling.

Furthermore, the addition of PEG polymer as an additive resulted in a reduction of the double-layer capacitance at the Zn surfaces (Fig. 3b). This decrease in double-layer capacitance is attributed to the adsorption of PEG polymer on the Zn anodes. As the molecular weight of PEG increases, a noticeable pattern emerges with a decrease in capacitance. The observed decrease in capacitance is associated with the homogeneous deposition of PEG molecules on the surface of zinc. This molecular deposition, in turn, reduces the formation of a direct double-layer surface between the zinc metal surface and zinc ions. Previous studies have emphasized the inhibitory effect of polymer adsorption on substrate surfaces, effectively mitigating dendrite growth during metal electrodeposition processes, including Zn electrodeposition [27, 37]. The presence of PEG polymer on Zn anodes facilitated the formation of a uniform and smooth Zn surface. Because of the interaction between ether groups ($–CH_2–O–CH_2–$) in the PEG polymer and Zn^{2+} ions, the interactions increase the concentration of Zn^{2+} ions near the Zn anode surface, which induces the uniform deposition of Zn^{2+}. This property could prevent random deposition and growth, thus contributing to a stable and even Zn deposition during repeated cycling.

To determine the influence of the molecular weight of PEG on the electrochemical stability of Zn, we used SEM to examine the morphology of the Zn anode after cycling. Figure 4 displays the SEM images of the Zn anode collected from a Zn || Zn symmetric cell after 20 cycles. In 1 M $ZnSO_4$ electrolytes, heterogeneous and porous Zn deposition was observed across a wide range of the Zn anode surface (Fig. 3a). The deposited Zn exhibited a tendency for vertical growth, resulting in an increased number of randomly exposed edges. Although sharp dendrites were not detected, the heterogeneity of the Zn deposition layer was found to increase gradually with repeated cycling. Over time, the initial Zn pre-dendrites transformed into critical Zn dendrites capable of breaching the separator and causing short-circuiting within the Zn || Zn cells, as depicted in Fig. 1a. With the addition of the PEG polymer, the morphologies of the deposited Zn exhibited increased flatness and homogeneity. This observation aligns with the significantly enhanced cycling performance of the Zn electrode when subjected to 1 M $ZnSO_4$ + 0.1 wt.% PEG electrolytes (Fig. 2a).

The surface roughness of the Zn anode after cycling appeared to be influenced by the molecular weight of PEG. Specifically, incorporating PEG300 into the electrolyte resulted in the formation of a highly homogeneous Zn anode surface (Fig. 4c). Following deposition in the presence of the PEG300 additive, no significant dendrite particles were observed on the Zn surface, and the electrode surface was coated with a compact layer of Zn particles with consistent sizes. This observation suggests effective control over the nucleation of Zn. The inclusion of PEG300 was observed to enhance the density of active sites and nucleation rate, leading to a significant increase in nucleation density. Consistent with the preceding electrochemical data, the PEG300 additive evidently exhibits low overpotential and robust inhibition properties toward H_2 evolution.

Conclusion

We have presented an effective approach for optimizing the interface of Zn anodes by carefully selecting the appropriate molecular weight of PEG. PEG in an aqueous electrolyte afforded a more uniform surface morphology of the Zn anode after cycling and acted as a protective layer against the generation of H_2 gas. Our findings demonstrate that the impact of PEG was significantly influenced by its specific molecular weight. The voltage hysteresis during Zn deposition–dissolution exhibited noticeable variations in PEG-containing electrolytes with different molecular weights. Through an investigation of the adsorption states of PEG with diverse molecular weights, we identified PEG300 as the most appropriate polymer. The electrochemical performance of Zn anodes in 1 M $ZnSO_4$ electrolytes with 0.1 wt.% PEG300 showed stable cycling over 232 cycles with high reversibility. By contrast, Zn anodes without the PEG300 additive-caused failure after 70 cycles in 1 M $ZnSO_4$ electrolytes. The results of this work provide valuable insight into the design and selection of highly effective additives to modify dilute salt electrolytes, enabling dendrite-free deposition on Zn anodes.

Acknowledgements The authors would like to thank the Cooperative Equipment Center at KOREATECH.

Funding This research was supported by the Chung-Ang University Research Scholarship Grants in 2022 and Technology development Program funded by Korea Government (MSS) (S3177328) and the Korea Institute of Energy Technology Evaluation and Planning (KETEP) funded by the Korea Government (MOTIE) (No. 20221B1010003A).

References

1. W. Kang, I. Nam, C. Jo, Korean J. Chem. Eng. **40**, 1353 (2023)
2. W. Nie, H. Cheng, Q. Sun, S. Liang, X. Lu, B. Lu, J. Zhou, Small Methods (2023). https://doi.org/10.1002/smtd.202201572
3. L. Ma, Q. Li, Y. Ying, F. Ma, S. Chen, Y. Li, H. Huang, C. Zhi, Adv. Mater. **33**, 2007406 (2021)
4. K. Zou, P. Cai, X. Deng, B. Wang, C. Liu, Z. Luo, X. Lou, H. Hou, G. Zou, X. Ji, Chem. Commun. **57**, 528 (2021)
5. Y.-F. Hu, L.-F. Zhou, H. Gong, H. Jia, P. Chen, Y.-S. Wang, L.-Y. Liu, T. Du, Korean J. Chem. Eng. **39**, 2353 (2022)
6. D. Han, S. Wu, S. Zhang, Y. Deng, C. Cui, L. Zhang, Y. Long, H. Li, Y. Tao, Z. Weng, Small **16**, 2001736 (2020)
7. M. Zhang, H. Hua, P. Dai, Z. He, L. Han, P. Tang, J. Yang, P. Lin, Y. Zhang, D. Zhan, J. Chen, Y. Qiao, C.C. Li, J. Zhao, Y. Yang, Adv. Mater. **35**, 2208630 (2023)
8. F. Yang, J.A. Yuwono, J. Hao, J. Long, L. Yuan, Y. Wang, S. Liu, Y. Fan, S. Zhao, K. Davey, Adv. Mater. **34**, 2206754 (2022)
9. Z. Guo, L. Fan, C. Zhao, A. Chen, N. Liu, Y. Zhang, N. Zhang, Adv. Mater. **34**, 2105133 (2022)
10. X. Zhang, J. Li, D. Liu, M. Liu, T. Zhou, K. Qi, L. Shi, Y. Zhu, Y. Qian, Energy Environ. Sci. **14**, 3120 (2021)
11. Y. Chu, S. Zhang, S. Wu, Z. Hu, G. Cui, J. Luo, Energy Environ. Sci. **14**, 3609 (2021)
12. Z. Xu, S. Jin, N. Zhang, W. Deng, M.H. Seo, X. Wang, Nano Lett. **22**, 1350 (2022)
13. M. Gopalakrishnan, S. Ganesan, M.T. Nguyen, T. Yonezawa, S. Praserthdam, R. Pornprasertsuk, S. Kheawhom, Chem. Eng. J. **457**, 141334 (2023)
14. X. Zeng, K. Xie, S. Liu, S. Zhang, J. Hao, J. Liu, W.K. Pang, J. Liu, P. Rao, Q. Wang, Energy Environ. Sci. **14**, 5947 (2021)
15. Z. Li, A.W. Robertson, Battery Energy **2**, 20220029 (2023)
16. C. Lin, X. Yang, P. Xiong, H. Lin, L. He, Q. Yao, M. Wei, Q. Qian, Q. Chen, L. Zeng, Adv. Sci. **9**, 2201433 (2022)
17. X. Yang, W. Li, J. Lv, G. Sun, Z. Shi, Y. Su, X. Lian, Y. Shao, A. Zhi and X. Tian, Nano Res. **15**, 9785 (2021)
18. Y. An, Y. Tian, Q. Man, H. Shen, C. Liu, Y. Qian, S. Xiong, J. Feng, Y. Qian, ACS Nano **16**, 6755 (2022)
19. X. He, Y. Cui, Y. Qian, Y. Wu, H. Ling, H. Zhang, X.-Y. Kong, Y. Zhao, M. Xue, L. Jiang, J. Am. Chem. Soc. **144**, 11168 (2022)
20. B.W. Olbasa, C.J. Huang, F.W. Fenta, S.K. Jiang, S.A. Chala, H.C. Tao, Y. Nikodimos, C.C. Wang, H.S. Sheu, Y.W. Yang, Adv. Func. Mater. **32**, 2103959 (2022)
21. K. Leng, G. Li, J. Guo, X. Zhang, A. Wang, X. Liu, J. Luo, Adv. Func. Mater. **30**, 2001317 (2020)
22. S. Guo, L. Qin, C. Hu, L. Li, Z. Luo, G. Fang, S. Liang, Adv. Energy Mater. **12**, 2200730 (2022)
23. Y. Dai, C. Zhang, W. Zhang, L. Cui, C. Ye, X. Hong, J. Li, R. Chen, W. Zong, X. Gao, Angew. Chem. Int. Ed. **62**, e202301192 (2023)
24. M. Wang, X. Wu, D. Yang, H. Zhao, L. He, J. Su, X. Zhang, X. Yin, K. Zhao, Y. Wang, Chem. Eng. J. **451**, 138589 (2023)
25. J. Cao, D. Zhang, X. Zhang, Z. Zeng, J. Qin, Y. Huang, Energy Environ. Sci. **15**, 499 (2022)
26. J. Zhou, H. Yuan, J. Li, W. Wei, Y. Li, J. Wang, L. Cheng, D. Zhang, Y. Ding, D. Chen, Chem. Eng. J. **442**, 136218 (2022)
27. Z. Cao, X. Zhu, S. Gao, D. Xu, Z. Wang, Z. Ye, L. Wang, B. Chen, L. Li, M. Ye, Small **18**, 2103345 (2022)
28. H. He, H. Qin, J. Wu, X. Chen, R. Huang, F. Shen, Z. Wu, G. Chen, S. Yin, J. Liu, Energy Storage Mater. **43**, 317 (2021)
29. S. Jin, Y. Deng, P. Chen, S. Hong, R. Garcia-Mendez, A. Sharma, N.W. Utomo, Y. Shao, R. Yang, L.A. Archer, Angew. Chem. Int. Ed. **62**, e202300823 (2023)
30. D.E. Ciurduc, C. de la Cruz, N. Patil, A. Mavrandonakis, R. Marcilla, Mater. Today Energy **36**, 101339 (2023)
31. M. Yan, C. Xu, Y. Sun, H. Pan, H. Li, Nano Energy **82**, 105739 (2021)
32. Y. Jin, K.S. Han, Y. Shao, M.L. Sushko, J. Xiao, H. Pan, J. Liu, Adv. Func. Mater. **30**, 2003932 (2020)
33. S. Jin, J. Yin, X. Gao, A. Sharma, P. Chen, S. Hong, Q. Zhao, J. Zheng, Y. Deng, Y.L. Joo, Nat. Commun. **13**, 2283 (2022)
34. G. Ma, L. Miao, Y. Dong, W. Yuan, X. Nie, S. Di, Y. Wang, L. Wang, N. Zhang, Energy Storage Mater. **47**, 203 (2022)
35. K. Zhao, F. Liu, G. Fan, J. Liu, M. Yu, Z. Yan, N. Zhang, F. Cheng, ACS Appl. Mater. Interfaces **13**, 47650 (2021)
36. M.N.C. Zarycz, C.F. Guerra, J. Phys. Chem. Lett. **9**, 3720 (2018)
37. A. Mitha, A.Z. Yazdi, M. Ahmed, P. Chen, ChemElectroChem **5**, 2409 (2018)